Behaviours of direct yellow 12 adsorption on mesoporous carbons with different pore geometries

Fengling Liu, Ziyan Guo, Hui Qiu, Xia Lu, Hua Fang and Jie Ren

ABSTRACT

Four kinds of mesoporous carbons, C1-h-w, C2-h-h, C3-s-w, and C4-s-h, with different pore geometries were prepared and characterised, and their adsorption behaviours with aqueous direct yellow 12 (DY-12) were investigated. The results of X-ray diffraction and transmission electron microscopy show that C1-h-w and C3-s-w have wormlike pore characteristics, whereas C2-h-h and C4-s-h have 2-D hexagonally arranged pores. According to the N_2 adsorption/desorption results, the specific surface area of C1-h-w (1,378 m^2/g) is the largest among the four carbons. The adsorption isotherms could be effectively fitted using the Langmuir model. The maximum adsorption amounts of C1-h-w, C2-h-h, C3-s-w and C4-s-h are 0.968 mmol/g, 0.726 mmol/g, 0.161 mmol/g and 0.156 mmol/g, respectively. The pseudo-second-order rate constants of C1-h-w (39.8 g/(mmol·min)) and C2-h-h (7.28 g/(mmol·min)) are substantially larger than those of C3-s-w (0.0046 g/(mmol·min)) and C4-s-h (0.014 g/(mmol·min)), indicating that an open and interconnected pore geometry is favourable for DY-12 adsorption. Furthermore, DY-12 diffusion in 2-D hexagonally ordered cylindrical pores is superior to that in wormlike pores due to the smoothness of the channels in the former. External mass transfer and intraparticle diffusion both play roles in the adsorption process.

Key words | adsorption, dye, mesoporous carbon, pore geometry

Fengling Liu (corresponding author)
Hua Fang
Collaborative Innovation Center of Atmospheric Environment and Equipment Technology,
Nanjing University of Information Science & Technology,
Nanjing 210044,
China
E-mail: *liufl@nuist.edu.cn*

Fengling Liu
Ziyan Guo
Hui Qiu
Xia Lu
Jie Ren
School of the Environmental Science & Engineering,
Nanjing University of Information Science & Technology,
Nanjing 210044,
China

Hui Qiu
Jiangsu Key Laboratory of Atmospheric Environment Monitoring and Pollution Control,
Nanjing University of Information Science & Technology,
Nanjing 210044,
China

INTRODUCTION

Ordered mesoporous carbons, which possess unique properties including high surface areas, tunable pore sizes, and alternative pore geometries as well as good chemical and mechanical stabilities, have attracted considerable interest in many fields, such as adsorption, separation, electrochemistry, catalysis, and energy storage. In aqueous environmental applications, ordered mesoporous carbons are usually used to remove organic pollutants such as natural organic matter, dyes, pharmaceuticals, and phenols (Ji *et al.* 2010; Tripathi *et al.* 2013; Yang *et al.* 2016; Chong *et al.* 2017). Excellent adsorption efficiencies are often reported for ordered mesoporous carbons, particularly in the case of contaminants with large molecular sizes (Ji *et al.* 2010; Tripathi *et al.* 2013; Chong *et al.* 2017).

The abundance of mesopores in porous carbons is well-known to play a very important role in the adsorption of bulky pollutants. Ip *et al.* reported that the adsorption capacity of mesoporous bamboo carbon for reactive black 5 was much higher than that of microporous activated carbon F400 (Ip *et al.* 2009). In addition, some researchers have noted that ordered mesoporous carbons with high specific surface areas and large pore volumes usually exhibit an excellent adsorption capacity and a fast adsorption rate for bulky rhodamine B (Tripathi *et al.* 2013). Furthermore, the adsorption properties of mesoporous carbons have also been affected by the sizes of their mesopores (Yuan *et al.* 2008; Puziy *et al.* 2016).

The pore geometry of ordered mesoporous carbons may also influence the adsorption properties of adsorbents. One of our previous studies reported that the open and interconnected pores of CMK-3 were more suitable for the adsorption of bulky reactive black 5 than the relatively closed and isolated pores of Si-CMK-5 (Liu *et al.* 2016). Libbrecht *et al.* reported that CMK-3, which has an open pore geometry consisting of interlinked nanorods, exhibited faster intraparticle diffusion and a higher removal rate of

doi: 10.2166/wst.2018.104

bisphenol-A than another mesoporous carbon with long cylindrical pores (Libbrecht *et al.* 2015). However, these articles discussed the influences of the pore geometry and pore connectivity of only 2-D hexagonally ordered mesoporous carbons, and other pore geometries, such as wormlike pores, were not mentioned.

In some studies, the authors noted that ordered mesoporous carbons with 2-D hexagonal symmetry exhibited the best supercapacitive performance because they possessed the fastest ion diffusion rate along the smooth channels relative to carbons with 3-D cubic mesopores and disordered wormlike characteristics (Sun *et al.* 2010; Liu & Zhang 2015). Thus, the diffusion rate of organic pollutant molecules is likely affected by the pore geometry. Additionally, the role that the geometry of the pore channels play in determining the adsorption behaviours of bulky organic pollutants such as dyes on mesoporous carbons with similar pore connectivity is not known, and this question has not yet been systematically discussed.

To clearly study the effects of the pore geometry on aqueous dye adsorption, four kinds of mesoporous carbons with diverse pore geometries were prepared by hard and soft templating methods and applied as adsorbents. Direct yellow 12 (DY-12), which is frequently used in the leather and paper industries, was selected as the adsorbate, and its molecular structure and properties are compiled in Figure S1. Schematic descriptions of the mesoporous structures of the selected adsorbents are displayed in Figure S2, and simple schematic descriptions of pore formation are also included to clearly show the connectivity of the pores. (Figures S1 and S2 are available with the online version of this paper.) The pores of the two hard-templated carbons are highly interconnected and open, while the other two soft-templated adsorbents have relatively isolated and closed pores. All of the adsorbents possess different pore structures and are expected to show varied adsorption affinities and adsorption kinetics towards DY-12.

EXPERIMENTAL

Preparation of hard silica templates

Mesoporous silica, SBA-15, was prepared according to the procedure reported by Zhao *et al.* (Zhao *et al.* 1998). Pluronic P123 was dissolved in an HCl solution at 40 °C before tetraethoxylsilane (TEOS) was added. The molar ratio of the reaction mixture was 1.00 TEOS: 0.017 P123: 7.5 HCl: 208 H_2O. After stirring at 40 °C for 24 h, the mixture was transferred to a Teflon-lined autoclave and heated at 100 °C for 48 h. The white precipitate was filtered, washed with distilled water, and dried at 80 °C overnight. The product was obtained after calcination at 550 °C for 6 h to remove the organic surfactant, Pluronic P123.

Hexagonal mesoporous silica (HMS) was synthesised according to the method described in the literature (Sevilla *et al.* 2004). Typically, the surfactant dodecylamine (DDA) was dissolved in ethanol, and a specific amount of water was added under vigorous stirring. After a homogeneous solution was obtained, TEOS was added, and the reaction solution was stirred at 40 °C for 24 h. The molar composition of TEOS/DDA/ethanol/H_2O was 1:0.27:6.5:36. Then, the mixture was filtered, washed with water and dried at 80 °C for 12 h. The surfactant was removed by calcination of the product at 650 °C for 4 h in air.

Preparation of mesoporous carbons

Two of the mesoporous carbons were prepared by a hard template method using SBA-15 and HMS, respectively, as the templates according to the references (Sevilla *et al.* 2004; Bazula *et al.* 2008). A furfuryl alcohol (FA) solution containing oxalic acid as a catalyst and having a volume equal to the pore volume of the structural mesopores was added to mesoporous silica SBA-15 or HMS. Then, the mixture was polymerised at 50 °C for 24 h and at 90 °C for another 24 h under air. The solid composites were heated at 150 °C for 3 h and carbonised at 850 °C for 4 h under vacuum. The carbon products were acquired after the residue was treated with 10% (wt) aqueous HF solution, washed with alcohol and distilled water and dried at 100 °C for 12 h. The carbon originating from HMS was designated C1-h-w, and the other carbon was denoted C2-h-h.

Two other carbons were synthesised using a structure-directing agent, triblock copolymer F127, as a soft template (Liu *et al.* 2010). Briefly, 6.78 g of resorcinol and 15 g of F127 were added to a mixture composed of 120 mL of distilled water and 120 mL of ethanol and stirred at room temperature. After the solid had dissolved completely and a colourless solution was obtained, 1.2 g of 37% HCl was added, and the mixture was stirred for 1 h. Then, 15 g of a formaldehyde solution was added dropwise to the above solution under vigorous stirring. A homogeneous yellowish solution was obtained after stirring for another 1 h, and this solution was transferred to a Teflon-lined autoclave, which was kept at 50 °C for 96 h. The hydrothermally treated sample was collected by filtration, washed with water and dried at 50 °C for 12 h, and then at 80 °C for another 12 h.

Finally, the sample was heated to 600 °C at a heating rate of 1 °C/min under a nitrogen atmosphere and kept at 600 °C for 6 h. The obtained carbon was ground, washed with ethanol and distilled water, and named C3-s-w. The mesoporous carbon, labeled C4-s-h, was obtained via the same synthetic procedure as that for C3-s-w, except the molar ratio of formaldehyde to resorcinol and the autoclaving period were changed to 2 h and 48 h, respectively. In the names of the four carbons, Cx-y-z, x stands for the number of a given carbon, y indicates the synthetic method (h is short for hard template and s is short for soft template), and z represents the pore geometry (h denotes 2-D hexagonal and w denotes wormlike).

Material characterisation

Powder X-ray diffraction (XRD) patterns of C1-h-w, C2-h-h, C3-s-w and C4-s-h were recorded on a Rigaku D/max-RA powder diffractometer (Rigaku, Tokyo, Japan) using Cu Kα radiation. Scanning electron microscopy (SEM) and transmission electron microscopy (TEM) images of the four adsorbates were taken on a Hitachi SU1510 scanning electron microscope (Hitachi Co. Ltd, Tokyo, Japan) and a JEM-200CX electron microscope, respectively. Elemental analyses of the four carbons were carried out with an elemental analyser of Heraeus CHN-O Rapid (Hanau, Germany) to determine the C, H, and N contents. The zeta potential (ζ) of the adsorbents was measured on a zeta potential analyser (Zeta PALS, Brookhaven Instruments Co., Holtsville, NY, USA). N_2 adsorption–desorption isotherms were collected on a Micrometrics ASAP 2020 apparatus (Micromeritics Instrument Co., Norcross, GA) at −196 °C (77 K).

Adsorption isotherms

Batch adsorption experiments were performed using 40 mL glass vials with polytetrafluoroethylene-lined screw caps. A weighed amount of adsorbent and a sufficient volume of distilled water were added to a glass vial, and then, a stock solution of DY-12 was added. The initial pH levels of the samples with C1-h-w and C2-h-h were in the range 7.8–9.1 and 7.4–8.7, respectively, and those of the samples with C3-s-w or C4-s-h were in the range 7.4–7.6. The C1-h-w and C2-h-h samples were shaken in a dark orbital shaker at 25 °C for 10 days, and the other carbons were shaken for 35 days. After filtration through a nylon fibre filter (0.45 μm), the filtrates were examined using a UV-visible spectrometer with a detection wavelength of 400 nm. The pH values of all the samples were measured at the end of the batch adsorption experiments, and a value of 7.0 ± 0.1 was obtained. In the control experiments conducted in the absence of an adsorbent, no loss of DY-12 was observed during the filtration and blank adsorption processes. The equilibrium adsorption amounts were calculated as follows:

$$q_e = (C_0 - C_e)V/M \quad (1)$$

where q_e is the equilibrium adsorption amount, C_0 is the initial solute concentration, C_e is the equilibrium concentration, V is the volume of solution and M is the mass of the adsorbent.

Adsorption kinetics

The kinetics of DY-12 adsorption on the tested materials were examined at an initial concentration of 0.073 mmol/L. Briefly, 100 mL of distilled water and a desired amount of adsorbent were first magnetically stirred in a 500 mL flask for approximately 20 min. Then, 400 mL of the aqueous solute was added and stirred in a dark isothermal incubator at 25 °C. Approximately 3 mL of the sample was removed from the suspension at different time intervals and filtered to measure the residual concentration.

RESULTS AND DISCUSSION

Characterisation

The small-angle XRD patterns of C1-h-w, C2-h-h, C3-s-w and C4-s-h are compiled in Figure S3 (available with the online version of this paper). C1-h-w, prepared using HMS as the hard template, shows a single diffraction peak, clearly reflecting the disordered wormlike pore structure of this material (Sevilla *et al.* 2004). For C2-h-h, a strong diffraction peak and two very weak peaks indicate the presence of 2-D hexagonal mesopore symmetry (Lee *et al.* 2002). The XRD pattern of C4-s-h displays a strong, narrow reflection peak, which is also indicative of an ordered 2-D hexagonal structure (Sun *et al.* 2010). For C3-s-w, the diffraction peak is much weaker than that for C4-s-h, indicating that the mesoporous structure of C3-s-w is more disordered than that of C4-s-h (Sun *et al.* 2010). Nevertheless, note that although the structures of C1-h-w and C3-s-w are disordered in the long range, the width of the pore channels is uniform. The differences in the regularity of the mesoporous structure between the four carbons can be further verified by examination of their TEM images in Figure 1. In the high

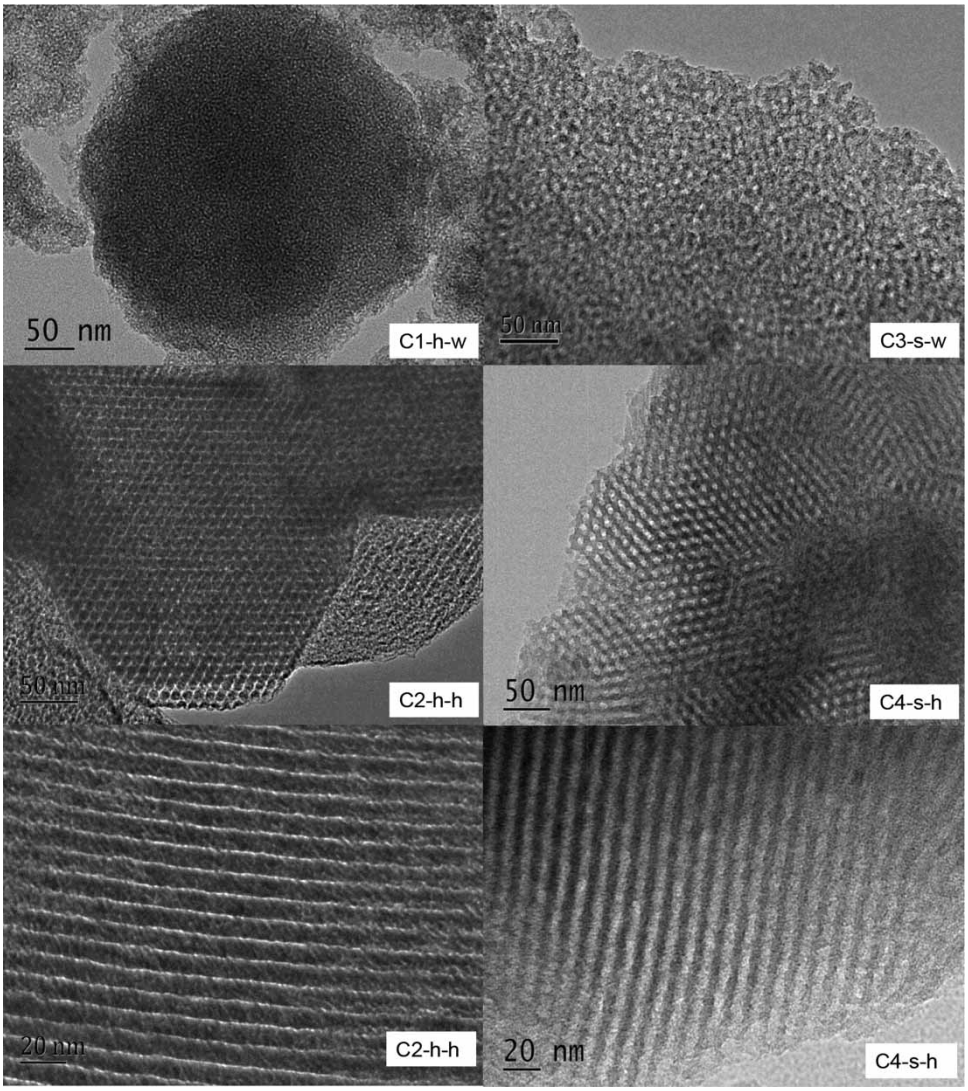

Figure 1 | Transmission electron microscopy images of the four carbons.

magnification images of C2-h-h and C4-s-h, the observation of parallel stripes with comparable distances confirms the long-range ordered arrangement of the mesopores. However, only disordered pore structures composed of short, wormlike mesoporous channels could be observed in the images of C1-h-w and C3-s-w. Moreover, the white circles around the dark dots in the low magnification images of C1-h-w and C2-h-h reflect the open pore structure of these materials. In contrast, the white dots of C3-s-w and C4-s-h that are encircled by dark skeletons are the projections of the closed pores. SEM images of the materials in Figure S4 show that the particle size of all the carbons is up to the micrometer scale. C3-s-w and C4-s-h take on smooth carpolite-like morphology while the surfaces of C1-h-w and C2-h-h particles seem to be rough. C2-h-h particles form via the aggregation of primary particles with rod-like morphology.

The zeta potential results in Figure S5 show that the isoelectric points (IEPs) of all the adsorbents are below 6. The isoelectric point of C3-s-w of approximately 2.5 is nearly the same as that of C4-s-h, as a result of the use of identical synthetic materials and thermal treatment procedures for these two carbons. The higher isoelectric point of C1-h-w (approximately 5.6) relative to that of C2-h-h (approximately 4.0) may be explained by the introduction of nitrogen-containing groups from the template for silica, 1-dodecylamine, which is further proven by the higher nitrogen content determined for C1-h-w than for the other carbons (Table S1). (Figures S4 and S5 and Table S1 are available online.)

Figure S6 (available online) shows the N_2 adsorption–desorption isotherms and pore size distributions of C1-h-w, C2-h-h, C3-s-w and C4-s-h. All four tested carbons exhibit a type IV isotherm (Figure S6(a)) with pronounced capillary condensation steps at $P/P_0 = 0.3$–0.8. These steps are ascribed to the mesopores in the carbon frameworks. However, unlike the other carbons, C1-h-w has an additional, clearer capillary condensation step at a high relative pressure, corresponding to the interparticle voids between the original particles (Sevilla *et al.* 2004). As seen in Table 1, a large pore volume remains in C1-h-w after deduction of the micropore and mesopore volumes, which could also result from the interspaces between the primary particles. Additionally, various characteristics of the pore size distributions of these carbons, calculated by the Barrett–Joyner–Halenda (BJH) method using the desorption branch, are shown in Figure S6(b). The pore diameter of C1-h-w centred at 2.3 nm is the smallest among the four and is sequentially followed by that of C2-h-h, C3-s-w, and C4-s-h. The narrow and mono-modal pore size distributions of C1-h-w and C3-s-w further illustrate the uniform width of their pore channels.

Adsorption isotherms

The adsorption isotherms of DY-12 with the equilibrium pH levels of 7.0 ± 0.1 are compiled in Figure 2. The data were fitted using the Langmuir adsorption model:

$$q_e = q_\infty b C_e / (1 + b C_e) \quad (2)$$

where q_∞ is the maximum adsorption amount and b is the Langmuir adsorption constant. The fitting parameters are summarised in Table 2. Generally, all the adsorption results

Table 1 | Pore structure parameters of C1-h-w, C2-h-h, C3-s-w, and C4-s-h

Adsorbent	D[a] (nm)	S_{BET}[b] (m^2/g)	V_T[c] (cm^3/g)	V_{micro}[d] (cm^3/g)	V_{BJH}[e] (cm^3/g)	V_{meso}[f] (cm^3/g)	V_{macro}[g] (cm^3/g)
C1-h-w	2.3	1378	2.99	0	3.10	1.85	1.25
C2-h-h	3.8	945	1.27	0.12	1.34	1.34	0
C3-s-w	4.3	659	0.63	0.03	0.52	0.52	0
C4-s-h	5.0	633	0.63	0.10	0.57	0.57	0

[a]Pore diameter calculated by BJH method.
[b]Specific surface area determined by N_2 adsorption using the Brunauer–Emmett–Teller (BET) method.
[c]Total pore volume determined at relative pressure $P/P_0 = 0.99$.
[d]Micropore volume estimated using t-plot method.
[e]The cumulative pore volume (pores 1.7–300 nm) calculated by BJH method.
[f]The cumulative mesopore volume (1.7 < pores < 50 nm) calculated by BJH method.
[g]The cumulative macropore volume (50 < pores < 300 nm) calculated by BJH method.

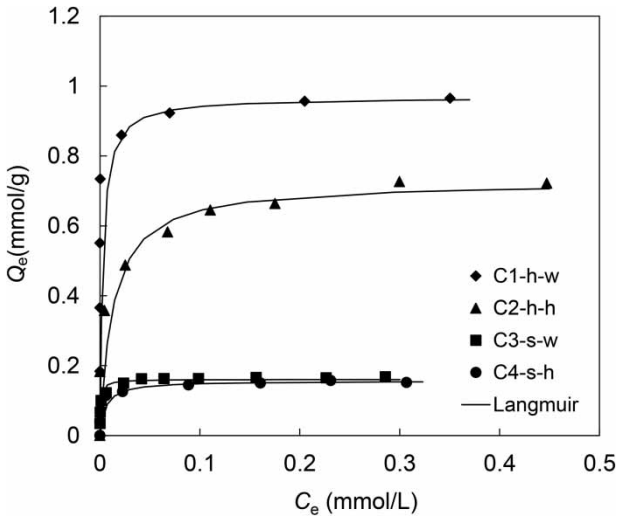

Figure 2 | Adsorption isotherms plotted as the solid-phase concentration (q_e) versus the aqueous-phase concentration (C_e) at the equilibrium of DY-12 adsorption for the different adsorbents with equilibrium pH values of 7.0 ± 0.1. Solid lines represent the fitting curves from the Langmuir adsorption model.

Table 2 | Fitting parameters of DY-12 adsorption on the tested carbons using the Langmuir model

Adsorbent	q_∞ (mmol/g)	b (L/mmol)	R^2
C1-h-w	0.968	356	0.988
C2-h-h	0.726	78	0.961
C3-s-w	0.161	1,221	0.996
C4-s-h	0.156	180	0.967

are effectively described by the Langmuir adsorption model, with $R^2 > 0.95$. The maximum adsorption amounts of the different adsorbents follow the order of C1-h-w > C2-h-h > C3-s-w, C4-s-h, revealing that the mesoporous carbons synthesised by the hard template method and containing open pore structures have stronger DY-12 adsorption abilities than the two carbons with relatively closed mesopore structures, C3-s-w and C4-s-h. The extremely high adsorption amount of C1-h-w indicates that C1-h-w has great potential for the removal of aqueous dyes. Li *et al.* also reported that the wormhole-structured mesoporous carbons synthesised using mesoporous silica as a template showed excellent adsorption capacities for amaranth and methylene blue (Li *et al.* 2011). Interestingly, the carbons with relatively closed mesopores have larger Langmuir adsorption constants (b) than those with open mesopores (C3-s-w > C1-h-w, C4-s-h > C2-h-h). Similar results were also found in our previous study (Liu *et al.* 2016). The larger b values reflect a stronger DY-12 adsorption affinity for the carbons with

closed pores than for those with open pores. The closed pores of C3-s-w and C4-s-h are completely encircled by the carbon skeleton, which likely results in a higher adsorption potential compared with that of the partially surrounded open pores of C1-h-w and C2-h-h. Additionally, the adsorption affinity of C1-h-w for DY-12 is strong, in contrast to that of C2-h-h, perhaps because of the small pore size of C1-h-w. This same trend also fits the comparison of C3-s-w with C4-s-h. Carbon is the major component of all the adsorbents, as shown in Table S1. C2-h-h and C4-s-h exhibit similar adsorption amounts of a small phenol after normalisation to the surface area (seen in Figure S7, available online). Therefore, the influences of the carbon surfaces, except charges on DY-12 adsorption are considered to be minor. The zeta potential results show that the surfaces of the tested adsorbents are negatively charged to different degrees. Hence, the disparity in adsorption patterns is probably due to the differences in the pore structures of the adsorbents and electrostatic repulsion.

To eliminate the effect of electrostatic repulsion on adsorption and clearly illustrate the role that the pore structure plays in adsorption, the adsorption isotherms with equilibrium pH levels equal to the IEP values of the adsorbents are compiled in Figure S8 (available online) and their surface area-based adsorption data (shown in Figure 3) were used for comparison. As seen in Figure S8, the differences in adsorption capacities between the four carbons are generally consistent with those with the equilibrium pH levels close to 7.0 (in Figure 2). After the adsorption capacities were normalised by the specific surface area of the adsorbents, C1-h-w and C2-h-h still exhibit much stronger adsorption abilities than C3-s-w and C4-s-h though the pore diameters of the former adsorbents are smaller than those of the latter ones. Considering that the molecular size of DY-12 is $2.94 \times 0.80 \times 0.57$ nm^3 (Chiang *et al.* 2009), the mesopores of the four adsorbents are fully accessible to the DY-12 molecules and, therefore, the pore size should not be the main factor that creates such adsorption differences. As seen from Figure S2, C1-h-w and C2-h-h, synthesised by the hard template method, possess open and interconnected mesoporous structures, while the pore structures of C3-s-w and C4-s-h are relatively closed and isolated. Such a sharp difference in the pore structures leads to entirely different access ability of the pores to the adsorbent. As noted in our previous study, for the carbons with open and interconnected pore channels, adsorbate molecules can enter the inner surface of the pores from a variety of directions (Liu *et al.* 2016). In contrast, for C3-s-w and C4-s-h, only the pore mouth at either end can be used as the entrances for molecules due to the closed and isolated structures. Thus, the pores of C3-s-w and C4-s-h are prone to blockage, which results in the inefficient adsorption of bulky DY-12. Between the two hard-templated carbons, C1-h-w shows slightly stronger adsorption at low concentrations of DY-12 than C2-h-h and slightly weaker adsorption at high concentrations, probably as a result of their different pore sizes. Just as mentioned above, the different adsorption patterns mainly result from the difference in the pore structures of the adsorbents. Adsorbents with small pore sizes are known to have strong adsorption potentials for adsorbates (Sastre *et al.* 1998; Yuan *et al.* 2008). C1-h-w with a small pore diameter is thought to possess strong adsorption potential which is beneficial for strong adsorption. Therefore, C1-h-w may be able to achieve a high adsorption amount when the DY-12 concentration is low. At high concentrations, the pore blockage effect is more likely to occur in the small pores and obstruct the entrances for the bulky DY-12 molecules into some of the adsorption sites in the deep channels. However, there is only a slight difference in the DY-12 adsorption capacity between C3-s-w and C4-s-h, indicating that the two closed pore channels with wormlike or cylindrical geometries have no influence on the DY-12 adsorption capacity.

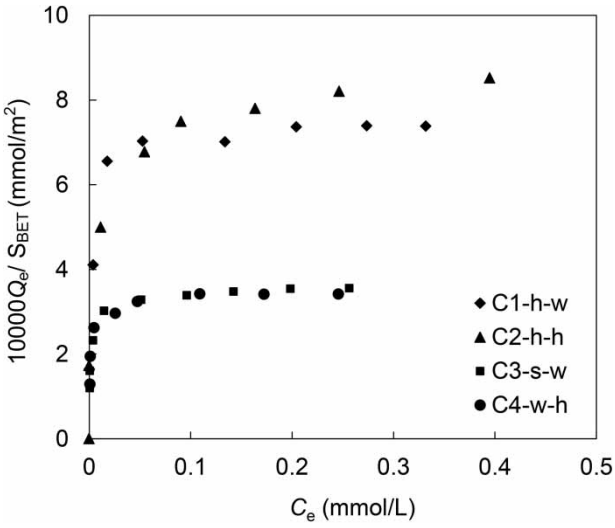

Figure 3 | Adsorption isotherms plotted as the surface area-based solid-phase concentration (q_e) versus the aqueous-phase concentration (C_e) at the DY-12 adsorption equilibrium for the different adsorbents with the equilibrium pH levels equal to the IEPs of the adsorbents.

Adsorption kinetics

The kinetics results of DY-12 adsorption on the tested adsorbents are compared in Figure 4. The mesoporous carbons synthesised using hard silica templates show

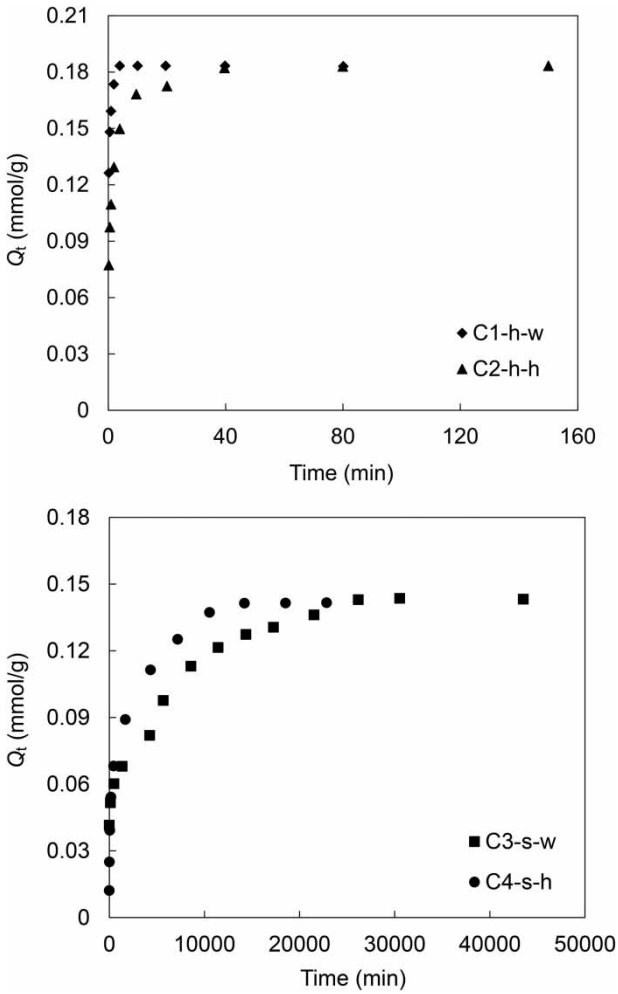

Figure 4 | Time-resolved adsorption of DY-12 on C1-h-w, C2-h-h, C3-s-w, and C4-s-h.

dramatically faster adsorption processes than the other two carbons with the same initial concentration. For example, C1-h-w and C2-h-h reached the adsorption equilibrium within 5 min and 40 min, respectively. However, approximately 26,200 min and 14,200 min were required to reach the adsorption equilibrium in the case of C3-s-w and C4-s-h, respectively, even though their adsorption amounts are lower than those of the former. Such a large gap in the adsorption rate between these carbons further reflects the absolute advantage of the tested hard-templated carbons in the removal of bulky dyes. Moreover, the carbons prepared by a given templating method also show different adsorption rates, namely, C3-s-w versus C4-s-h and C1-h-w versus C2-h-h.

The pseudo-first-order and pseudo-second-order kinetics models (Trivedi *et al.* 1973; Ho & McKay 1999), shown in Equations (3) and (4), respectively, were used to evaluate the mass transfer during the DY-12 adsorption process.

$$\log(q_e - q_t) = \log(q_e) - k_1 t/2.303 \quad (3)$$

$$t/q_t = 1/(k_2 q_e^2) + t/q_e \quad (4)$$

In these equations, k_1 and k_2 are the pseudo-first-order rate constant and the pseudo-second-order rate constant, respectively.

The experimental data before the adsorption equilibrium were used to evaluate the adsorption kinetics because the data after the equilibrium have no influence on adsorption kinetics. The simulation results based on the pseudo-first-order and pseudo-second-order models are compiled in Figures S9 and S10, respectively (available online), and the fitting parameters are listed in Table 3. The simulation results suggest that pseudo-first-order kinetics model does not effectively describe the adsorption process of DY-12 adsorption on the four carbons. In contrast, the plots of t/q_t versus t give a linear relation with R^2 values above 0.99. Additionally, the adsorption amounts determined from the fitting results are nearly identical to those obtained from the experimental data, further indicating that the process of DY-12 adsorption on the tested carbons follows pseudo-second-order kinetics. As shown in Table 3, the adsorption rate constants of C1-h-w, C2-h-h, C3-s-w, and C4-s-h were calculated to be 39.8, 7.28, 0.0046, and 0.014 g/(mmol·min), respectively, indicating that these carbons possess significantly different adsorption rates.

Table 3 | Parameters for fitting the adsorption kinetics of C1-h-w, C2-h-h, C3-s-w, and C4-s-h by the pseudo-first-order and pseudo-second-order models

		Pseudo-first order kinetics			Pseudo-second order kinetics		
Adsorbent	**q_{exp} (mmol/g)**	**k_1 (min^{-1})**	**q_{cal} (mmol/g)**	**R^2**	**k_2 (g/(mmol·min))**	**q_{cal} (mmol/g)**	**R^2**
C1-h-w	0.183	1.1470	0.080	0.993	39.8000	0.186	1
C2-h-h	0.183	0.0950	0.071	0.940	7.2800	0.184	1
C3-s-w	0.144	0.0001	0.106	0.932	0.0046	0.144	0.986
C4-s-h	0.144	0.0002	0.095	0.962	0.0140	0.144	0.997

As discussed in the section on the adsorption isotherms, DY-12 adsorption is mainly affected by the pore structural properties of these carbons under our experimental conditions. The pore size may play a negligible role in determining the rate of DY-12 adsorption on the carbons in this study, as deduced from the adsorption results combined with the pore structures of the adsorbents. For example, C1-h-w has the fastest adsorption rate even though its pore diameter is the smallest. The pore diameter of C4-s-h is larger than that of C2-h-h, yet DY-12 adsorption on C4-s-h is much slower than that on C2-h-h. The suitable specific surface area or mesopore volume of the adsorbents seems to be one of the main reasons for the large differences in the adsorption rates. A high suitable specific surface area or mesopore volume corresponds to a large probability of contact with the molecules without influence from the pore size. At a low initial DY-12 concentration (0.073 mmol/L), the amount of completely unoccupied adsorption sites far exceeds the amount required for adsorption of the DY-12 molecules, and the steric hindrance effect is absent during adsorption. Hence, the DY-12 molecules may preferentially reach the adsorption sites in the regions around the pore mouths quickly and freely. Similar results were also observed in previous studies (Gupta *et al.* 2011; Liu *et al.* 2012). In addition, the pore geometry is another important factor that affects the DY-12 adsorption rate. In fact, the adsorption rate of C2-h-h with open and interconnected pore channels is overwhelmingly superior to that of C4-s-h with a closed and cylindrical pore structure because of the different diffusion paths of these two materials, which may be responsible for the large difference between the two carbons (Liu *et al.* 2016). Note that the effect of the pore channel geometry on the diffusion rate is clearly illustrated by the distinct adsorption rates of C3-s-w and C4-s-h. The long-range ordered and smooth channels of C4-s-h facilitate the diffusion of DY-12 molecules in the pores, while diffusion of the molecules in the disordered and wormlike pore channels of C3-s-w is likely to be hindered to some extent. Previous studies have also reported that a 2-D hexagonal pore symmetry is more favorable for diffusion than 3-D and disordered wormlike pore characteristics (Sun *et al.* 2010; Liu & Zhang 2015).

Generally, a solid–liquid adsorption process involves external mass transfer and intraparticle diffusion. To further verify the mechanism and rate-controlling steps in the adsorption process, the Weber-Morris model was used to evaluate intraparticle diffusion (Weber & Morris 1964):

$$q_t = k_d t^{1/2} + I \tag{5}$$

In this equation, k_d is the intraparticle diffusion constant and I is the intercept related to the diffusion boundary layer thickness. The plots of q_t versus $t^{1/2}$ are compiled in Figure S11 (available online), and the parameters are shown in Table 4. All the q_t–$t^{1/2}$ plots of the carbons except that of C1-h-w show two linear portions. All of the first linear portions deviate from the origin, reflecting the involvement of external mass transfer (Liu *et al.* 2012). The first linear portion is indicative of dye molecule diffusion in the pores of the adsorbent, and the second portion describes the final equilibrium step, during which intraparticle diffusion gradually slows down because of the greatly reduced concentration difference. The reason for the lack of the second linear portion of C1-h-w is not clear. Perhaps because of the very short time required to reach equilibrium in C1-h-w (less than 5 min), the second equilibrium step for this material is difficult to distinguish from the whole adsorption process, which consists of limited data points. Additionally, the carbons derived from hard templates show much higher K_{d1} values than the soft-templated carbons, suggesting markedly faster rates of DY-12 diffusion in the pores of the hard-templated carbons.

CONCLUSIONS

In the present study, four mesoporous carbons prepared by templating methods were examined to investigate the effects of the pore geometry on the adsorption of aqueous DY-12. All the adsorption isotherms of the carbons with DY-12 are effectively described using the Langmuir model. C1-h-w has the highest adsorption ability among the four tested adsorbents because it has the largest specific surface area and pore volume. Based on the surface-area-normalised

Table 4 | Kinetic parameters obtained with the Weber-Morris model

Adsorbent	k_{d1} (mmol/(g·min$^{1/2}$))	I_1 (mmol/g)	R^2	k_{d2} (mmol/(g·min$^{1/2}$))	I_2 (mmol/g)	R^2
C1-h-w	0.0508	0.1049	0.960	–	–	–
C2-h-h	0.0480	0.0580	0.972	0.0044	0.1539	0.980
C3-s-w	0.0006	0.0440	0.972	0.0005	0.0655	0.960
C4-s-h	0.0051	0.0073	0.991	0.0008	0.0507	0.971

adsorption isotherms, C1-h-w and C2-h-h with open and interconnected pores synthesised by the hard template method show much stronger DY-12 adsorption than the soft-templated carbons, C3-s-w and C4-s-h, whose pores are relatively closed and isolated. These results indicate that the connectivity of the pores and the pore geometry strongly affect DY-12 adsorption. The good match in the adsorption isotherms between C1-h-w and C2-h-h and between C3-s-w and C4-s-h reveal that the geometry of the pore channels has no effect on DY-12 adsorption. However, the adsorption kinetics results reveal that the rate of DY-12 adsorption is strongly influenced by the geometry of the pore channels as well as their connectivity. DY-12 adsorption on C1-h-w and C2-h-h is far more rapid than that on C3-s-w and C4-s-h. Furthermore, due to its smooth and straight channels, C4-s-h with 2-D hexagonal symmetry has a higher adsorption rate than C3-s-w with disordered and wormlike pore characteristics.

ACKNOWLEDGEMENTS

The study was financially supported by the National Natural Science Foundation of China (Nos 51608277 and 21607080) and the Natural Science Foundation of Jiangsu province (No. BK20160946). This work was also supported by the Project Funded by the Priority Academic Program Development of Jiangsu Higher Education Institutions (PAPD), Jiangsu Engineering Technology Research Center of Environmental Cleaning Materials.

REFERENCES

Bazula, P. A., Lu, A. H., Nitz, J. J. & Schüth, F. 2008 Surface and pore structure modification of ordered mesoporous carbons via a chemical oxidation approach. *Microporous and Mesoporous Materials* **108** (1–3), 266–275.

Chiang, H. M., Chen, T. C., Pan, S. D. & Chiang, H. L. 2009 Adsorption characteristics of Orange II and Chrysophenine on sludge adsorbent and activated carbon fibers. *Journal of Hazardous Materials* **161** (2–3), 1384–1390.

Chong, Y. P., Liu, K., Liu, Y., Wang, J. T., Qiao, W. M., Ling, L. C., Long, D. H. & Bai, Z. S. 2017 Highly efficient removal of bulky tannic acid by millimeter-sized nitrogen-doped mesoporous carbon beads. *AIChE Journal* **63** (7), 3016–3025.

Gupta, V. K., Gupta, B., Rastogi, A., Agarwal, S. & Nayak, A. 2011 A comparative investigation on adsorption performances of mesoporous activated carbon prepared from waste rubber tire and activated carbon for a hazardous azo dye – acid blue 113. *Journal of Hazardous Materials* **186** (1), 891–901.

Ho, Y. S. & McKay, G. 1999 Pseudo-second-order model for sorption processes. *Process Biochemistry* **34** (5), 451–465.

Ip, A. W. M., Barford, J. P. & McKay, G. 2009 Reactive black dye adsorption/desorption onto different adsorbents: effect of salt, surface chemistry, pore size and surface area. *Journal of Colloid and Interface Science* **337** (1), 32–38.

Ji, L. L., Liu, F. L., Xu, Z. Y., Zheng, S. R. & Zhu, D. Q. 2010 Adsorption of pharmaceutical antibiotics on template-synthesized ordered micro- and mesoporous carbons. *Environmental Science & Technology* **44** (8), 3116–3122.

Lee, J. S., Joo, S. H. & Ryoo, R. 2002 Synthesis of mesoporous silicas of controlled pore wall thickness and their replication to ordered nanoporous carbons with various pore diameters. *Journal of the American Chemical Society* **124** (7), 1156–1157.

Li, J. T., Li, B. L., Wang, H. C., Bian, X. B. & Wang, X. M. 2011 A wormhole-structured mesoporous carbon with superior adsorption for dyes. *Carbon* **49** (6), 1912–1918.

Libbrecht, W., Vandaele, K., Buysser, K., Verberckmoes, A., Thybaut, J. W., Poelman, H., Clercq, J. & Voort, P. V. 2015 Tuning the pore geometry of ordered mesoporous carbons for enhanced adsorption of bisphenol-A. *Materials* **8** (4), 1652–1665.

Liu, Y. R. & Zhang, J. 2015 Influence of pore symmetries on the supercapacitive performance of mesoporous carbons co-templated by f127 and PDMS–PEO. *Microporous and Mesoporous Materials* **206**, 81–85.

Liu, L., Wang, F. Y., Shao, G. S. & Yuan, Z. Y. 2010 A low-temperature autoclaving route to synthesize monolithic carbon materials with an ordered mesostructure. *Carbon* **48** (7), 2089–2099.

Liu, F. L., Guo, Z. B., Zheng, S. R. & Xu, Z. Y. 2012 Adsorption of tannic acid and phenol on mesoporous carbon activated by CO_2. *Chemical Engineering Journal* **183**, 244–252.

Liu, F. L., Guo, Z. B., Ling, H. G., Huang, Z. N. & Tang, D. Y. 2016 Effect of pore structure on the adsorption of aqueous dyes to ordered mesoporous carbons. *Microporous and Mesoporous Materials* **227**, 104–111.

Puziy, A. M., Poddubnaya, O. I., Derylo-Marczewska, A., Marczewski, A. W., Blachnio, M., Tsyba, M. M., Sapsay, V. I. & Klymchuk, D. O. 2016 Kinetics of protein adsorption by nanoporous carbons with different pore size. *Adsorption -Journal of the Iinternational Adsorption Society* **22** (4–6), 541–552.

Sastre, G., Raj, N., Catlow, R. A., Roque-Malherbe, R. & Corma, A. 1998 Selective diffusion of C8 aromatics in a 10 and 12 MR zeolite. A molecular dynamics study. *The Journal of Physical Chemistry B* **102** (17), 3198–3209.

Sevilla, M., Alvarez, S. & Fuertes, A. B. 2004 Synthesis and characterization of mesoporous carbons of large textural porosity and tunable pore size by templating mesostructured HMS silica materials. *Microporous and Mesoporous Materials* **74** (1–3), 49–58.

Sun, G. W., Wang, J. T., Liu, X. J., Long, D. H., Qiao, W. M. & Ling, L. C. 2010 Ion transport behavior in triblock copolymer-templated ordered mesoporous carbons with different pore

symmetries. *The Journal of Physical Chemistry C* **114** (43), 18745–18751.

Tripathi, P. K., Liu, M. X., Gan, L. H., Qian, J. S., Xu, Z. J., Zhu, D. Z. & Rao, N. N. 2013 High surface area ordered mesoporous carbon for high-level removal of rhodamine B. *Journal of Materials Science* **48** (22), 8003–8013.

Trivedi, H. C., Patel, V. M. & Patel, R. D. 1973 Adsorption of cellulose triacetate on calcium silicate. *European Polymer Journal* **9** (6), 525–531.

Weber, W. J. & Morris, J. C. 1964 Removal of biologically resistant pollutants from waste waters by adsorption. In: *Advances in Water Pollution Research*, Vol. 2 (W. W. Eckenfelder, ed.), Pergamon Press, Oxford, UK, pp. 231–266.

Yang, B., Liu, Y. P., Li, Z. J., Lei, L. C., Zhou, J. & Zhang, X. W. 2016 Preferential adsorption of pentachlorophenol from chlorophenols-containing wastewater using N-doped ordered mesoporous carbon. *Environmental Science and Pollution Research* **23** (2), 1482–1491.

Yuan, X., Xing, W., Zhuo, S. P., Si, W. J., Gao, X. L., Han, Z. H. & Yan, Z. F. 2008 Adsorption of bulky molecules of nonylphenol ethoxylate on ordered mesoporous carbons. *Journal of Colloid and Interface Science* **322** (2), 558–565.

Zhao, D. Y., Feng, J. L., Huo, Q. S., Melosh, N., Fredrickson, G. H., Chmelka, B. F. & Stucky, G. D. 1998 Triblock copolymer syntheses of mesoporous silica with periodic 50 to 300 angstrom pores. *Science* **279**, 548–552.

First received 5 August 2017; accepted in revised form 21 February 2018. Available online 5 March 2018